Optics & Laser Technology 181 (2025) 111673

Contents lists available at ScienceDirect

Optics and Laser Technology

journal homepage: www.elsevier.com/locate/optlastec

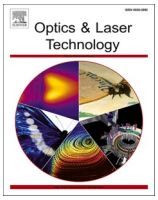

Full length article

Enhanced SERS performance of Ag nanoparticles using hybrid dewetting process for melamine detection

H.K. Lin [a,*], Yu-Ming Ding [a], Wei-I Yen [a], Chien-Hsing Chen [b], Jia-Ren Lee [c]

[a] Department of Materials Engineering, National Pingtung University of Science and Technology, Pingtung, Taiwan
[b] Department of Biomechatronics Engineering, National Pingtung University of Science and Technology, Pingtung, Taiwan
[c] Department of Physics, National Kaohsiung Normal University, Kaohsiung, Taiwan

ARTICLE INFO

Keywords:
Hybrid dewetting
Laser
Surface plasmon resonance
SERS

ABSTRACT

A thermal evaporation system was used to deposit Ag thin films on glass substrates. The films were dewetted using both a regular laser irradiation approach and a hybrid dewetting process that involved laser irradiation followed by Ag thermal deposition. The study would evaluate and compare the optical characteristics and efficiency in melamine detection within these dewetted films. In the traditional dewetting process, as the laser power increased from 15 to 25 W, the nanoparticles (NPs) size decreased from 162 to 125 nm. Furthermore, an evident optical absorption peak range of 540–600 nm was also observed. Through the hybrid dewetting process, a mixture of small NPs (20 nm) and larger NPs (142–167 nm) were formed. It resulted in two distinct Surface Plasmon Resonance (SPR) peaks at 460 nm and 660 nm, respectively. Notably, a strong Raman peak at 701 cm^{-1} emerged when a melamine aqueous solution was placed on the hybrid dewetted surface. Comparing the two methods, the hybrid dewetted sample exhibited enhanced fingerprint peak intensity and a higher analytical enhancement factor (AEF). When operating at laser power of 25 W and a scanning speed of 100 mm/s, the maximum AEF value reached 1.9×10^5. The limit of detection for melamine solution in the hybrid dewetted sample was established at 10^{-7} M. Hence, the hybrid dewetting process is a potential method to produce the mixed-sized nanoparticles for diverse applications.

1. Introduction

Melamine is recognized for its high hardness, exceptional heat resistance, and effective flame retardancy. This has led to its widespread utilization in creating melamine tableware, thermosetting coatings, flame-retardant blankets, and other applications. Furthermore, melamine is commonly incorporated into food products as a preservative. Despite its relatively low toxicity, prolonged consumption of melamine can result in various negative health outcomes, including the development of kidney stones, bladder cancer, and other ailments [1]. As a consequence, many studies have witnessed some significant methods to determine the melamine concentration within foods and beverages, particularly within the realm of food safety and monitoring. Several techniques are available for melamine detection, such as high-performance liquid chromatography ultraviolet spectrometry (HPLC/UV), liquid chromatography-tandem mass spectrometry (LC-MS/MS), and gas chromatography-mass spectrometry (GC/MS) [2]. Among these methods, Raman spectrometry could be as a prominently utilized technique. This approach captures the vibration spectrum of a distinct molecule or lattice. When coupled with the detection of nanoparticles (NPs), it gives rise to a methodology referred to as surface-enhanced Raman scattering (SERS) [3,4]. Raman spectroscopy offers a rapid and efficient means of melamine detection and is characterized by a distinct peak at 682 cm^{-1} in the Raman spectrum, often referred to as the melamine fingerprint peak [5–13].

Nanoparticles (NPs) exhibit a multitude of unique attributes, encompassing enhanced surface plasmon resonance (SPR) effects [14] and remarkable antimicrobial efficacy [15]. The resonant traits of NPs exhibit wide variations contingent upon their composition, morphology, and dimensions [16]. Nowadays, nanoparticles applications includes antibiotics [17,18], biomedicine [19,20], optoelectronics [21], and Raman spectroscopic analysis [13,22]. Noble metal nanoparticles like gold, silver, and copper have attracted significant interest owing to their strong surface plasmon resonance (SPR) effects and noteworthy electrical field characteristics [23]. The signal enhancement mechanism of SERS is mainly considered to include both electromagnetic

* Correspondent author.
E-mail address: HKLin@mail.npust.edu.tw (H.K. Lin).

https://doi.org/10.1016/j.optlastec.2024.111673
Received 2 January 2024; Received in revised form 5 July 2024; Accepted 20 August 2024
Available online 29 August 2024

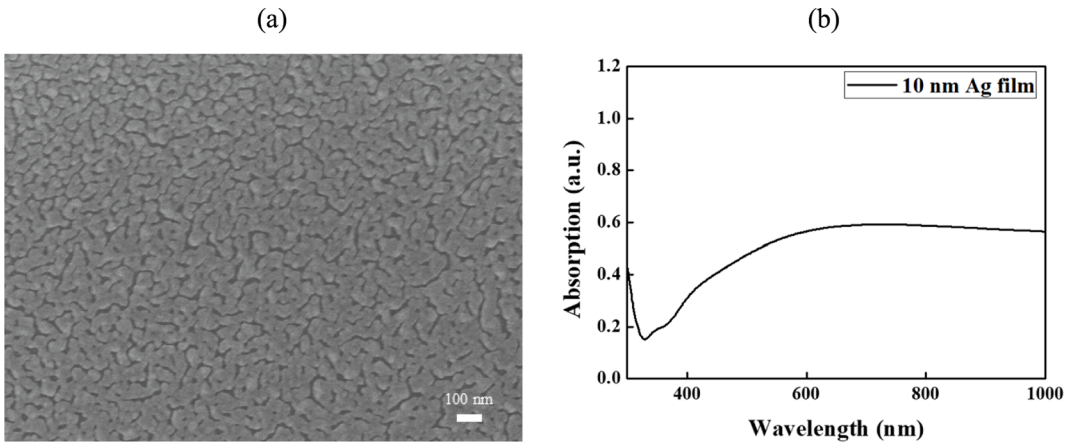

Fig. 1. (a) SEM image and (b) absorption spectrum of 10-nm Ag film deposited on glass.

enhancement and chemical enhancement [24]. Among them, electromagnetic enhancement exhibits a greater enhancement amplitude [25]. Plasmonic sensors are used to monitor changes in local refractive index or spectral fingerprints to detect analytes. The strong EM field in metallic nanostructures can enhance the Raman signals of the target molecules nearby, making them more easily identifiable, and it has lower detection limits compared to other detection techniques [26]. These EM fields primarily originate from nanogaps in metallic structures or structural hotspots, also known as EM hotspots [27]. Several research studies have demonstrated that narrowing the gap in metal nanostructures creates hotspots, resulting in the generation of a strong electromagnetic field [28,29].

Additionally, they amplify the hotspot effect in Surface-Enhanced Raman Scattering, thus finding extensive use in medical diagnostics [30], and monitoring food safety [31]. Nanoparticles can be generated through several methods, including hydrothermal processes [32], chemical synthesis [33], methanol catalysis [34], and laser-induced dewetting [17,18,35–37]. However, nanoparticles produced through chemical processes often demonstrate inadequate adhesion to substrates. On the other hand, the resulting nanoparticles frequently exhibit incomplete crystal growth [38]. As a result, the utilization of dewetting methods to prompt the creation of small particles or nanostructures on the substrate surface has gained more attentions [35,39]. Conventional physical dewetting approaches tend to be time-consuming and lead to uneven distributions of nanoparticle sizes [39]. In contrast, laser-induced dewetting due to its localized heating impact, provides a straightforward, convenient, and cost-effective avenue for generating nanoparticles with customizable attribution [17,18,37].

The literature contains various investigations on the laser-driven dewetting strategies, encompassing the dewetting of films on pre-patterned substrates [40,41], the dewetting of template-confined films [42,43], and the dewetting of thin films by exploiting nanoscale Rayleigh-Taylor instabilities [44–46]. Moreover, several studies showed the application of laser-induced dewetting in the fabrication of biomedical tools [17,18], Raman detection [13], and surface plasmon resonance [37]. These studies have demonstrated the potential for the expansion of the laser dewetting technique into diverse domains [13]. However, based on current knowledge, the utilization of laser-induced dewetting to amplify the Surface-Enhanced Raman Scattering intensity signal in melamine detection remains largely unexplored.

Accordingly, the present study commences by depositing Ag thin films on glass substrates using a thermal evaporation technique. The films are dewetted via both a regular laser irradiation and a hybrid dewetting process consisting laser irradiation followed by thermal deposition. The nanostructures, size distribution, optical attributes, and melamine detection capabilities of the dewetted films are investigated through the two distinct approaches, thereby facilitating a comprehensive comparison.

2. Materials and methods

Glass substrates were initially cleaned by de-ionized water and dried with hot air, and then transferred to a thermal evaporator system (SSI-T500-1, Taiwan). The chamber's base pressure was established at 5×10^{-6} Torr before the deposition process. In the chamber, silver pellets were placed into a tungsten boat, where they were heated to vaporization using a resistive heat source. The growth conditions of the resulting silver film on the glass substrate were controlled by adjusting the current (I_{Ag}) and the time of the evaporation process. Specifically, I_{Ag} was maintained at 40 A, and the deposition rate was roughly 1 Å/sec, yielding silver thin films of approximately 10 nm and 2 nm, respectively.

After the deposition process, two distinct dewetting processes were employed for the silver films: (1) a traditional dewetting method involving laser irradiation, and (2) a hybrid dewetting process involving laser irradiation followed by Ag film deposition using the thermal evaporator system. In both cases, a continuous wave (CW) laser system (R4 HS Series, SPI) emitting at 1070 nm with a spot size of 19 μm was used for irradiation process. The laser power settings were adjusted to 15, 20, and 25 W, while the scanning speed was set at 100, 200, and 300 mm/s. In the hybrid dewetting process, these specific thermal evaporation conditions were established to deposit a 2 nm-thick silver film onto the dewetted film. The size and quantity of nanoparticles (NPs) formed were determined using ImageJ software (National Institutes of Health, USA). The spectrophotometer (Lambda 35, U.S.A) was employed to assess the absorbance properties of both the film in its original deposition state and the dewetted silver films. The suitability of the dewetted silver samples for Raman detection was evaluated using aqueous melamine solutions at concentrations ranging from 10^{-3} to 10^{-7} M. Furthermore, the Micro Raman system (MRI532S, Taiwan) with a wavelength of 532 nm was utilized to capture the Raman spectra of the melamine across different dewetted silver films.

The Discrete Dipole Approximation (DDA) involves the combination of numerous dipoles to form different waveforms, where the electric fields generated by these dipoles are superimposed and the extinction spectra of different waveforms are calculated. In DDA, an object is discretized into a set of small cubic units, with each unit being affected by incident waves, becoming polarized, and generating an electromagnetic field. To compute the electric field at each unit's position, considering the coupling between discretized elements, one must solve a linear system in the following form:

$$\mathbf{E} = \mathbf{E}\mathrm{ref} + \mathbf{AD}\alpha\mathbf{E} \quad (1)$$

$$(\mathbf{I} - \mathbf{AD}\alpha)\mathbf{E} = \mathbf{E}\mathrm{ref} \quad (2)$$

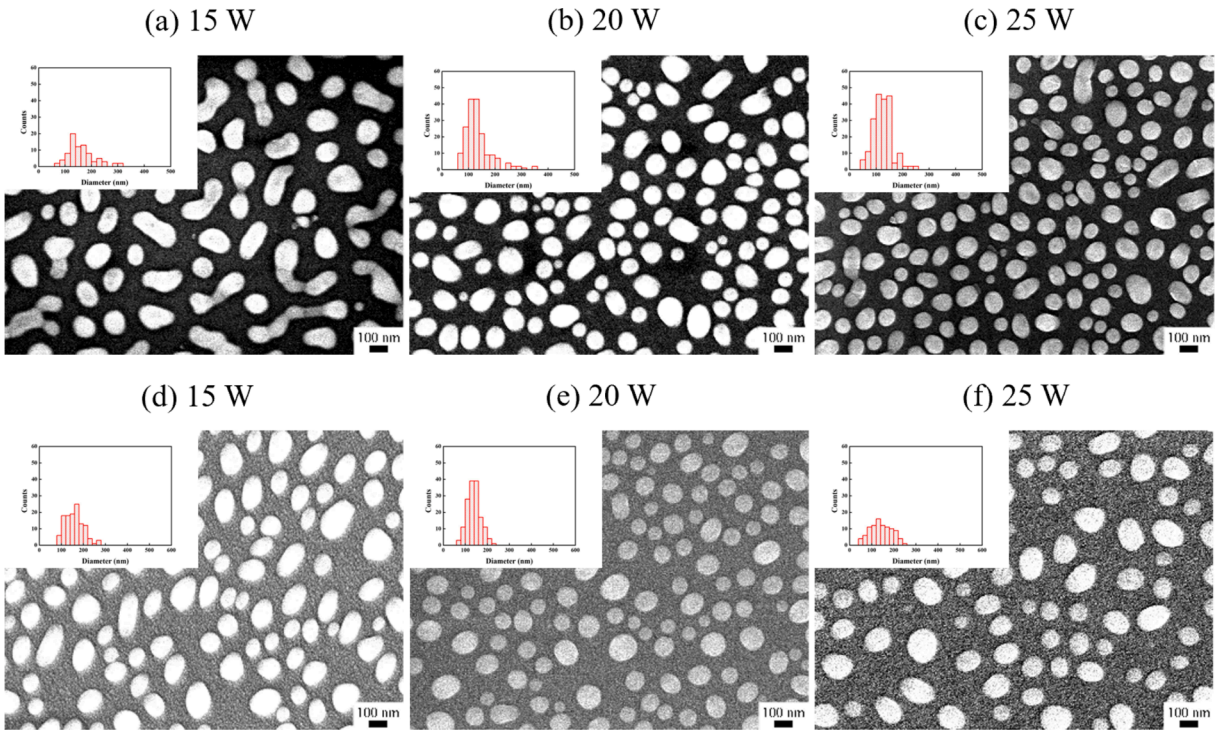

Fig. 2. (a)-(c) SEM morphologies and NP size distributions of dewetted films processed with scanning speed of 100 mm/s and laser powers of 15, 20, and 25 W, respectively; (d)-(f) hybrid dewetted samples.

Here, **A** is a ($3N \times 3N$) matrix containing all the Green's tensors, **E** and **E**ref are vectors of size $3N$, comprising the local field at each discretized element's position and the reference field (i.e., the field in the absence of the object), respectively. **D**α is a ($3N \times 3N$) diagonal matrix containing the polarizability of each unit, **I** is the identity matrix.

3. Results and discussions

3.1. Surface morphology and the formation of nanoparticles of laser irradiation and hybrid dewetting process

Fig. 1(a) shows the surface morphology of the 10-nm silver film deposited by thermal evaporation method. No obvious NPs could be observed. Thus, the absorption spectrum of the 10-nm deposited silver film shows in Fig. 1(b) reveals that the film has no LSPR effect. The 10-nm Ag thin film exhibits an absorption intensity of only 0.6 a.u at the incident wavelengths of 600–1000 nm. It means that the formation of nanoparticles is required to improve the light absorption performance of the film.

Fig. 2(a)–(c) show the surface morphologies and nanoparticle size distributions of the films irradiated by laser powers 15, 20 and 25 W, respectively. The 15 W-dewetted sample presents a small number of isolated island structures compared to the higher laser powers of 20 and 25 W. These films fully dewetted into high roundness nanoparticles. As the laser power increased from 15 to 25 W at scanning speed at 100 mm/s, the NP size decreased from 162 to 125 nm. During the dewetting process, the metal film undergoes melting due to the heat supplied by a laser, resulting in its disintegration. The metal then rapidly solidifies under cooling conditions. To minimize the total energy of the free surfaces of the film and substrate, as well as their interface, a spontaneous self-assembly of nanoparticles occurs. At a laser power of 15 W, the dewetted silver film has an island-like structure, indicating insufficient energy to fully form nanoparticles. As the laser power increases to 20 and 25 W, the dewetted silver film transforms into nanoparticle formations, with a corresponding decrease in particle size and improvement in morphology. This observed variation in particle morphology with increasing laser power has also been documented in previous studies [13,47].

Fig. 2(d)–(f) show the surface morphologies and nanoparticles size distributions of the hybrid dewetted samples. For the sample irradiated with a laser power of 15 W, the NP size increases slightly from 162 nm to 167 nm following the deposition of the additional silver layer with a thickness of 2 nm. In contrast to the traditional dewetting process, the NP size in the hybrid dewetted sample remains approximately unchanged as the laser power increases. Fig. 3(a) and (b) show the morphologies and NP size distributions of a thickness 2-nm silver film deposited on a glass slide and the hybrid dewetted sample processed at laser irradiated power of 25 W and a scanning speed of 100 mm/s. For the 2-nm silver film, the average particle size is around 20 nm. However, for the hybrid dewetted sample, the silver film contains a mixture of small and large NPs with a size of around 20 nm and 142–167 nm.

3.2. Absorption spectra of dewetted Ag films

Absorption spectra of the dewetted films are presented in Fig. 4(a)–(c), depicting various resulting from different scanning speeds (100, 200, and 300 mm/s) and laser powers (15, 20, and 25 W). All of the samples have a strong surface plasmon resonance peak at wavelength of 540–600 nm. A weak SPR peak is also observed at lower wavelengths of 350–370 nm. The nanoparticles (NPs) exhibit uniformity within the particle's electromagnetic field, resulting in the emergence of the primary dipole-type oscillation surface plasmon resonance (SPR) peak. However, a phase delay stimulates higher-order multipolar resonances, giving rise to the appearance of multiple SPR peaks in the spectrum [48,49]. It is seen in Fig. 4(a)~(c) that the peak wavelength reduces with an increasing power or a decreasing scanning speed, indicating a blue shift of the spectrum.

Fig. 4(d)~(f) show that absorption spectra of the hybrid dewetted samples with a 2-nm silver layer deposited on the dewetted surface. As shown in the three figures, the original silver film deposited directly on a glass substrate has a strong absorption peak at around 460 nm.

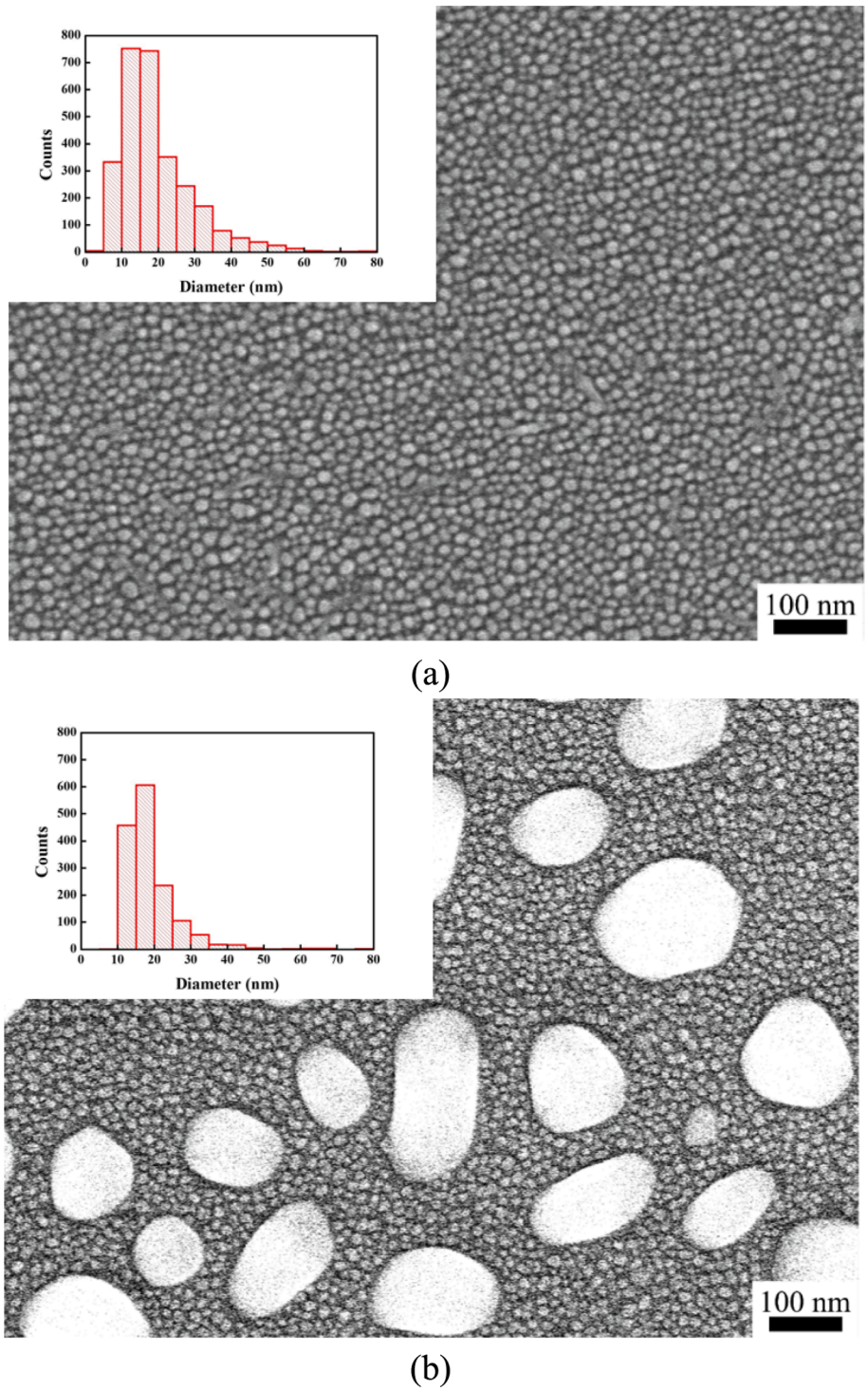

Fig. 3. Morphologies and size distributions of: (a) 2-nm Ag film deposited on glass, and (b) hybrid dewetted sample processed with scanning speed of 100 mm/s and laser power of 25 W.

However, the hybrid dewetted samples show an additional SPR peak in the range of wavelength 600–660 nm. In other words, the hybrid dewetted films exhibit two SPR peaks due to the presence of NPs with two different sizes in the dewetted morphology, namely 20 nm and 142–167 nm. Overall, the results show that the hybrid dewetting process leads to a broader SPR peak. Furthermore, the larger size of the NPs in the hybrid dewetted samples gives rise to a red shift of the spectrum.

3.3. *Melamine Raman detection of dewetted Ag films*

The Raman spectra of detecting aqueous melamine solution at concentration of 10^{-3} M placed in contact with the dewetted and hybrid dewetted films prepared with laser powers of 15, 20 and 25 W and a fixed scanning speed of 100 mm/s, respectively. For the dewetted films, no obvious peaks are observed for any of the dewetted films (Fig. 5(a)–(c)). However, a strong fingerprint peak at 701 cm^{-1} is observed for each of the hybrid dewetted samples (Fig. 5(d)–(f)). Moreover, it is seen that

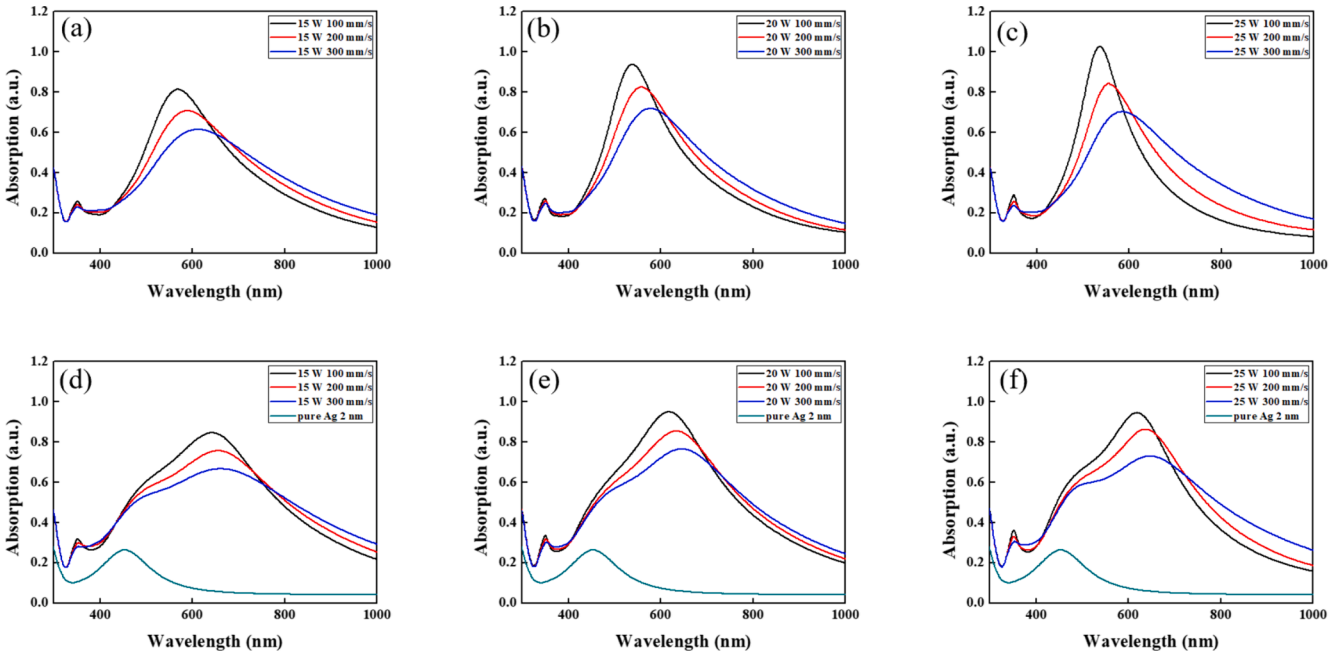

Fig. 4. Absorption spectra of: (a-c) dewetted Ag films, and (d)~(f) hybrid dewetted films. (Note that for both series of films, dewetting was performed using scanning speeds of 100–300 mm/s and laser powers of 15, 20, and 25 W, respectively. (Note also that the absorption spectrum of a 2-nm Ag film deposited on glass is shown in Fig. 4(d)~(f) for reference purposes.)

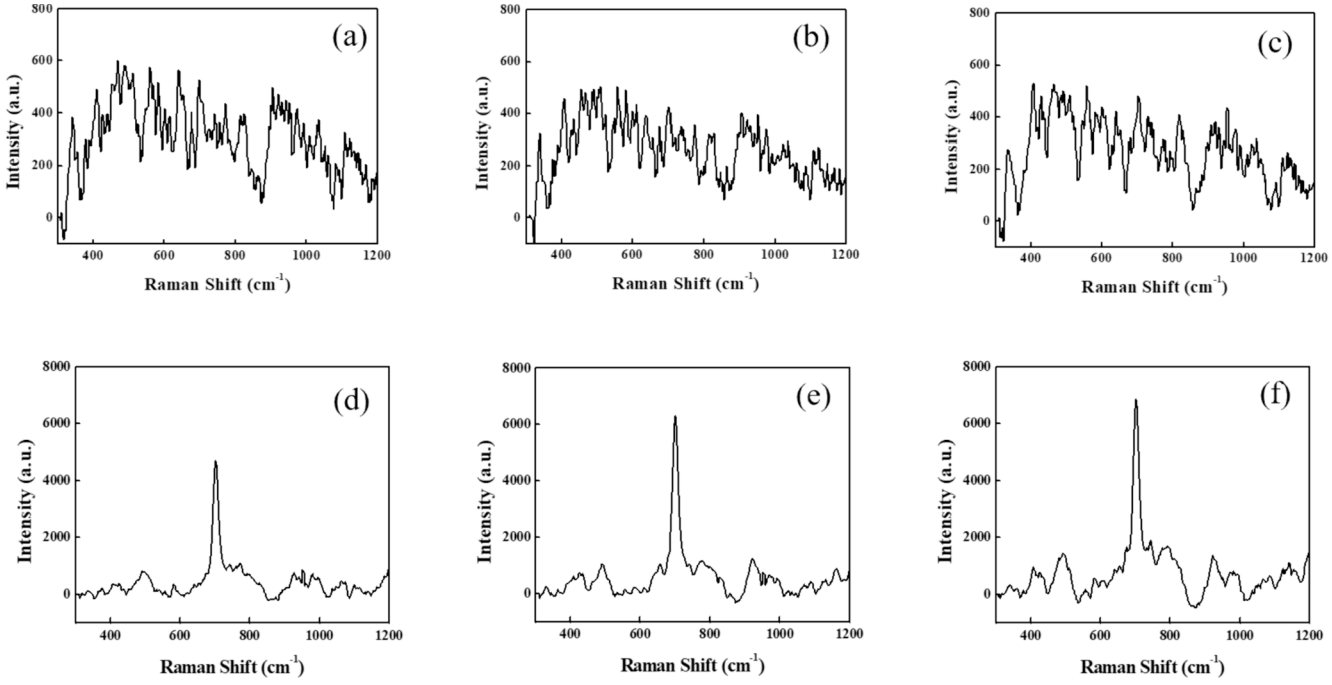

Fig. 5. Raman spectra for 10^{-3} M melamine solutions on: (a)~(c) dewetted Ag films, and (d)~(f) hybrid dewetted films. (Note that for both series of films, dewetting was performed using a scanning speed of 100 mm/s and laser powers of 15, 20, and 25 W, respectively.)

the hybrid dewetting sample can cause a stronger Raman signal of melamine than the traditional dewetting processes for all values of the irradiation power due to the mixed-size NP structure of the hybrid dewetted films. Although the larger particles exhibit LSPR performance, they are ineffective in detecting melamine due to the presence of gaps between particles. However, the smaller particles occupy these gaps and create additional hotspots that enhance the electromagnetic field, thus improving the melamine detection signal. Essentially, the smaller particles in the background provide supplementary hotspots that enhance the Raman signal of melamine. In the SERS process, the enhancement performance is greatly influenced by the hot spot. The SERS primary factors influencing the SERS hotspot are the excitation wavelength and the shape and size of the nanoparticles [50,51]. In other words, the size distribution of the particles on the substrate for SERS has a significantly impact on the intensity of the Raman signal. Hence, in the present study, the hybrid dewetted films show a stronger SPR and Raman enhancement than the dewetted films. It can be attributed to the amplified electromagnetic field and resonance quality that produced by the mixed

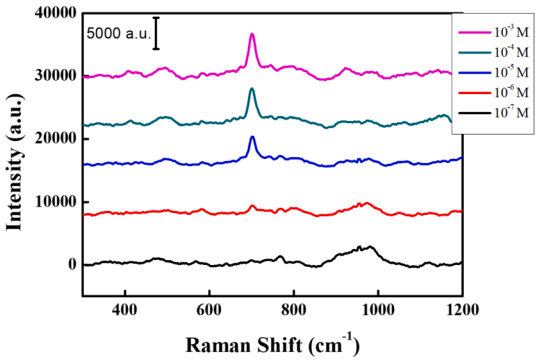

Fig. 6. LOD values for different melamine concentrations using hybrid dewetted sample processed with a scanning speed of 100 mm/s and laser power of 25 W.

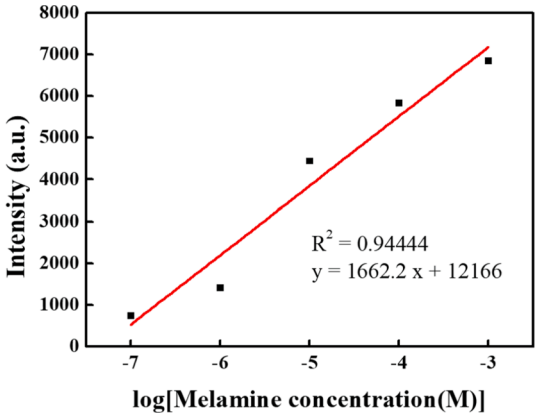

Fig. 7. Variation of Raman intensity with melamine concentration for hybrid dewetted sample processed with a scanning speed of 100 mm/s and laser power of 25 W.

particle size.

Fig. 6 shows the Raman spectra acquired from melamine with different concentrations in contact with the hybrid dewetted sample irradiated using with a laser power of 25 W and scanning speed of 100 mm/s. Peaks in the Raman spectra are observed for all of the considered melamine concentrations (10^{-3} to 10^{-7} M). Nevertheless, the fingerprint peak intensity at 701 cm^{-1} weakens as the concentration of melamine reduces, and a weak fingerprint signal still observed when the concentration reaches 10^{-7} M. In other words, the limit of detection (LOD) of the hybrid sample for melamine is 10^{-7} M. The LOD at 10^{-7} M is 0.0126 ppm, which is well below the safety limit of 2.5 ppm established by the United States and the European Union. Fig. 7 shows the variation of the Raman intensity with the melamine concentration for the hybrid dewetted sample. It is seen that the intensity decreases with a decreasing concentration.

The LOD enhancement of the hybrid dewetted sample compared to that of a regular laser irradiation sample can be evaluated via the following analytical enhancement factor (AEF):

$$AEF = (I_{SERS}/C_{SERS})/(I_{RS}/C_{RS}) \quad (3)$$

where I_{SERS} is the Raman intensity of the SERS enhanced signal, C_{SERS} is the melamine concentration associated with I_{SERS}. I_{RS} is the intensity of the signal without SERS enhancement, and C_{RS} is the melamine concentration associated with I_{RS}. The AEF value of the hybrid dewetted sample is found to be 1.9×10^5 for dewetting parameters of a laser power of 25 W and scanning speed of 100 mm/s.

Fig. 8(a) shows the SERS spectra obtained for a 10^{-3} M concentration of melamine solution in contact with the hybrid dewetted sample processed at 25 W and 100 mm/s. It is seen that for 10 randomly chosen points on the sample surface, the characteristic peak is located in the vicinity of 701 cm^{-1}. According to the analysis results presented in Fig. 8 (b), the relative standard deviation (RSD) of the 10 peak intensity measurements is just 4.37 %. In other words, the hybrid sample provides a feasible and stable substrate for melamine detection purposes.

The electric field interactions and electromagnetic field enhancements provided by the spacing between prepared nanoparticles are simulated by the DDA method. These different particle sizes and spacings are formed by varying dewetting parameters. Three structural configurations (Laser irradiation, 2 nm silver film deposition, and Hybrid dewetting) include a particle size of 134.4 nm with a spacing of 60 nm, a particle size of 20 nm with a spacing of 2 nm, and a mixed particle size of 144 nm and 20 nm with a spacing of 20 nm, respectively. Fig. 9(a)–(c) show the simulation results calculated using incident light wavelength at 532 nm. It's evident that the electronic field intensity is highly dependent on the gap distance. The simulation results clarify that in the case of laser dewetting alone, where the distance between particles is relatively large, the value of $|E|^2$ is smaller, leading to a less significant enhancement in SERS. However, when incorporating 2 nm silver film deposition with larger particles, the extremely close spacing between the small particles generates the strong hotspot enhancement. The presence of these small particles also compensates for the insufficient spacing between large particles to form hotspots, thereby creating EM hotspots and further enhancing the Raman signal of melamine when analyzing the hybrid dewetting sample as SERS substrate.

Fig. 10 presents a schematic diagram of the conventional dewetting process (I) and hybrid dewetted process (II). For illustration purposes, the dewetting process is assumed to be conducted using a laser power of

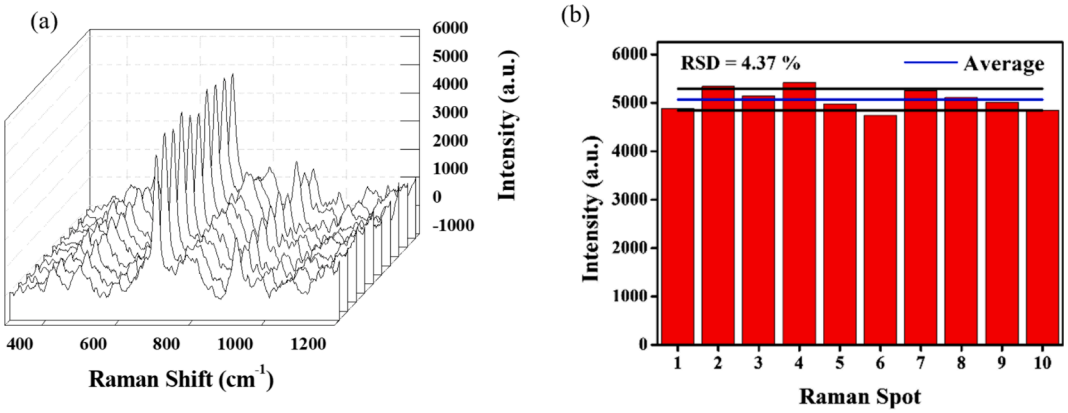

Fig. 8. (a) Melamine SERS spectra collected from 10 random points, and (b) relative standard error of Raman intensity at 701 cm^{-1} peak for hybrid dewetted sample processed at 25 W and 100 mm/s.

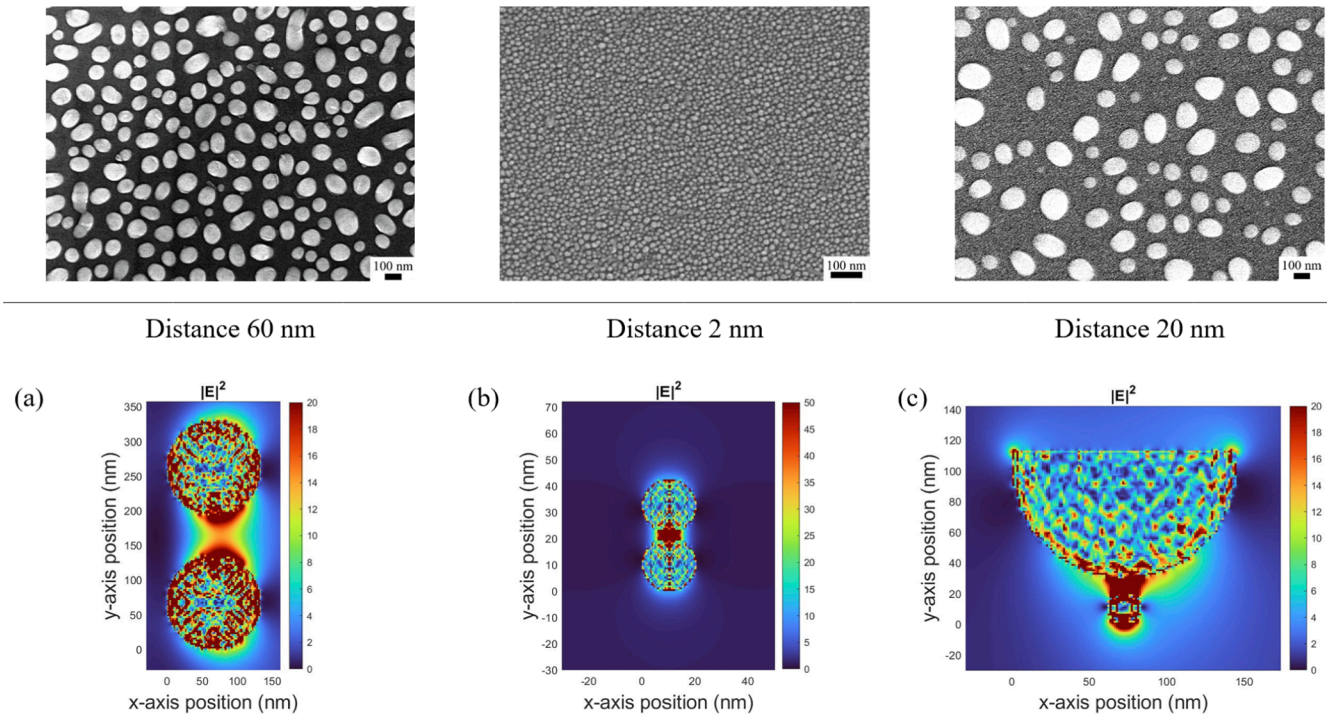

Fig. 9. SEM image and the simulated electromagnetic field intensity $|E|^2$ at (a) laser irradiation process, (b) 2 nm silver film deposition, and (c) Hybrid dewetting process.

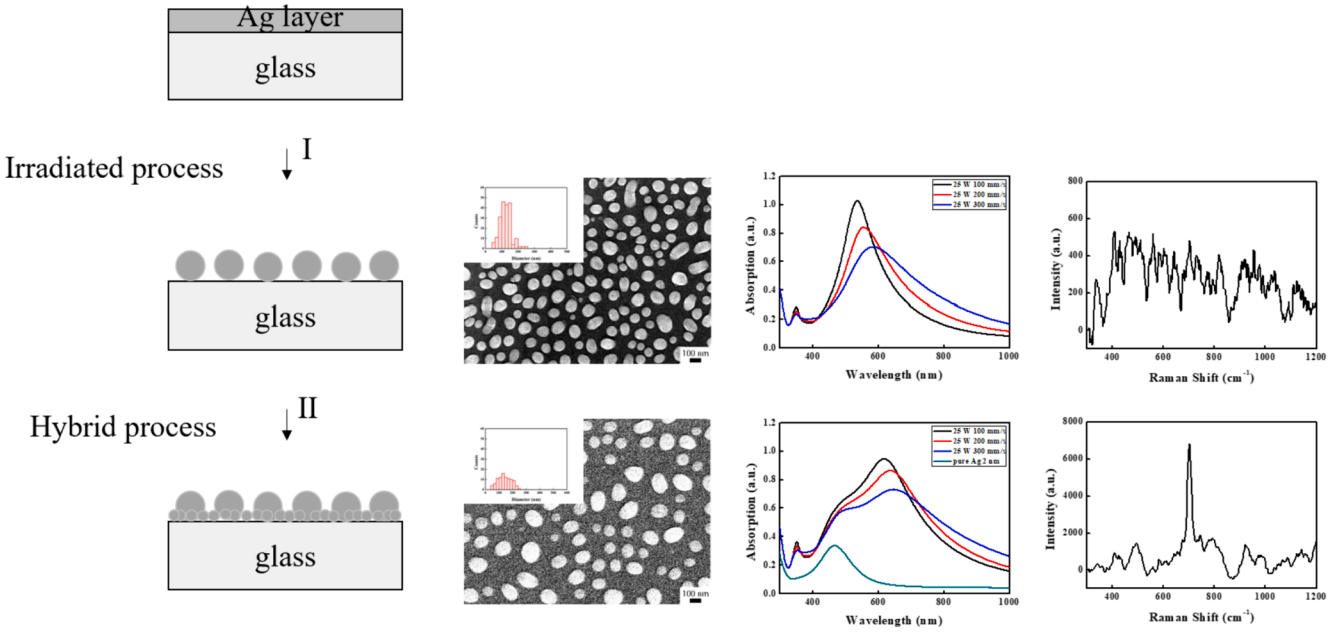

Fig. 10. Schematic diagrams of (I) laser irradiation process and (II) hybrid dewetted process, together with corresponding SEM morphologies, absorption spectra, and Raman spectra.

25 W. In the SEM images, the formed NPs in both cases have a larger and more uniform size. Moreover, the hybrid dewetted sample contains both large and small nanoparticles densely distributed on the surface. The SPR peak for the hybrid dewetted sample has a broader range (460–660 nm) than the traditional dewetted sample (540–600 nm). Finally, compared to the traditional dewetted sample, the hybrid sample exhibits a single obvious peak in the Raman intensity spectra. Thus, the hybrid dewetting process effectively enhances the LOD performance of the sample for melamine.

4. Conclusions

This study revealed the effects of two dewetting procedures (i.e., traditional laser irradiation and laser irradiation followed by thermal deposition) on the formation of NPs in thin Ag films deposited on glass substrates. In the traditional laser irradiation dewetting process, nanoparticles with a size of 162 and 125 nm were performed at laser powers of 15 and 25 W, respectively. Although the larger particles exhibit LSPR performance, they are ineffective in detecting melamine due to the

presence of gaps between particles. For the hybrid dewetted films, a mixture of small-sized (~20 nm) and large-sized nanoparticles with a size of 142–167 nm was formed at 25 W. The mixed-sized nanoparticles in the hybrid dewetted films led to an increase in the intensity of the SPR peak signal and a wider absorbance spectrum. The absorbance wavelength of the LSPR in the hybrid dewetted sample was from 460 to 660 nm, and it exhibited a red shift with a decreasing power. The smaller particles occupy these gaps and create additional hotspots that enhance the electromagnetic field, thus improving the melamine detection signal. Essentially, the smaller particles in the background provide supplementary hotspots that enhance the Raman signal of melamine. Based on these simulation results, when incorporating 2 nm silver film deposition with larger particles, the extremely close spacing between the small particles generates strong hotspot enhancement. The presence of these small particles also compensates for the insufficient spacing between large particles to form hotspots, thereby creating EM hotspots and further enhancing the Raman signal. When utilized for melamine detection, the hybrid dewetted sample displayed a more consistent fingerprint peak, a lower detection limit of 10^{-7} M, and a higher AEF of 1.9×10^5. Therefore, the hybrid dewetting process is a promising method for creating uniform mixed-sized nanoparticles for diverse applications.

CRediT authorship contribution statement

H.K. Lin: Writing – review & editing, Writing – original draft, Supervision, Resources, Investigation, Conceptualization. **Yu-Ming Ding:** Methodology, Formal analysis, Data curation. **Wei-I Yen:** Software, Methodology, Data curation. **Chien-Hsing Chen:** Visualization, Software. **Jia-Ren Lee:** Methodology, Formal analysis.

Declaration of competing interest

The authors declare that they have no known competing financial interests or personal relationships that could have appeared to influence the work reported in this paper.

Data availability

Data will be made available on request.

Acknowledgements

The authors gratefully acknowledge the financial support provided to this study by the National Science and Technology Council, ROC, under Project No. NSTC 112-2637-E-020-004.

References

[1] C.G. Skinner, J.D. Thomas, J.D. Osterloh, Melamine toxicity, J. Med. Toxicol. 6 (1) (2010) 50–55.
[2] P. Lutter, M.-C. Savoy-Perroud, E. Campos-Gimenez, L. Meyer, T. Goldmann, M.-C. Bertholet, P. Mottier, A. Desmarchelier, F. Monard, C. Perrin, F. Robert, T. Delatour, Screening and confirmatory methods for the determination of melamine in cow's milk and milk-based powdered infant formula: validation and proficiency-tests of ELISA, HPLC-UV, GC-MS and LC-MS/MS, Food Control 22 (6) (2011) 903–913.
[3] M. Fleischmann, P.J. Hendra, A.J. McQuillan, Raman spectra of pyridine adsorbed at a silver electrode, Chem. Phys. Lett. 26 (2) (1974) 163–166.
[4] D. Graham, The next generation of advanced spectroscopy: surface enhanced Raman scattering from metal nanoparticles, Angew. Chem. Int. Ed. Engl. 49 (49) (2010) 9325–9327.
[5] T.H. Chang, Y.C. Chang, C.M. Chen, K.W. Chuang, C.M. Chou, A facile method to directly deposit the large-scale Ag nanoparticles on a silicon substrate for sensitive, uniform, reproducible and stable SERS substrate, J. Alloy. Compd. 782 (2019) 887–892.
[6] K. Ge, Y. Hu, Y. Zheng, P. Jiang, G. Li, Aptamer/derivatization-based surface-enhanced Raman scattering membrane assembly for selective analysis of melamine and formaldehyde in migration of melamine kitchenware, Talanta 235 (2021) 122743.
[7] M. Tiwari, A. Singh, S. Dureja, S. Basu, S.K. Pattanayek, Au nanoparticles decorated ZnO/ZnFe(2)O(4) composite SERS-active substrate for melamine detection, Talanta 236 (2022) 122819.
[8] B. Nie, Y. Luo, J. Shi, L. Gao, G. Duan, Bowl-like Pore array made of hollow Au/Ag alloy nanoparticles for SERS detection of melamine in solid milk powder, Sens. Actuators B 301 (2019) 127087.
[9] C. Huang, S. Jiang, F. Kou, M. Guo, S. Li, G. Yu, B. Zheng, F. Xie, C. Zhang, H. Yu, J. Wang, Development of jellyfish-like ZnO@Ag substrate for sensitive SERS detection of melamine in milk, Appl. Surf. Sci. 600 (2022) 154153.
[10] G. Xiao, L. Li, A. Yan, X. He, Direct detection of melamine in infant formula milk powder solution based on SERS effect of silver film over nanospheres, Spectrochim. Acta A Mol. Biomol. Spectrosc. 223 (2019) 117269.
[11] C. Zhang, T. You, N. Yang, Y. Gao, L. Jiang, P. Yin, Hydrophobic paper-based SERS platform for direct-droplet quantitative determination of melamine, Food Chem. 287 (2019) 363–368.
[12] R. Li, J. Yang, J. Han, J. Liu, M. Huang, Quantitative determination of melamine in milk using Ag nanoparticle monolayer film as SERS substrate, Physica E 88 (2017) 164–168.
[13] H.K. Lin, T.Y. Li, I.C. Chen, Y.C. Lo, Laser-induced surface plasmon resonance and SERS performance of AgCuAl medium entropy alloy films, Mater. Lett. 333 (2023) 133701.
[14] S. Linic, U. Aslam, C. Boerigter, M. Morabito, Photochemical transformations on plasmonic metal nanoparticles, Nat. Mater. 14 (6) (2015) 567.
[15] M. Rai, A. Yadav, A. Gade, Silver nanoparticles as a new generation of antimicrobials, Biotechnol. Adv. 27 (1) (2009) 76–83.
[16] K.L. Kelly, E. Coronado, L.L. Zhao, G.C. Schatz, The Optical Properties of Metal Nanoparticles: The Influence of Size, Shape, and Dielectric Environment, ACS Publications, 2003.
[17] Y.H. Lin, J.J. Wang, Y.T. Wang, H.K. Lin, Y.J. Lin, Antifungal properties of pure silver films with nanoparticles induced by pulsed-laser dewetting process, Appl. Sci. 10 (7) (2020) 2260.
[18] J.J. Wang, H.K. Lin, W.S. Chuang, C.Y. Chuang, Y.H. Lin, J.C. Huang, Y.H. Lin, Laser dewetting mechanism and antibacterial properties of Cu-Al based medium entropy alloy films, J. Alloy. Compd. 903 (2022) 163893.
[19] H.-W. Chen, K.C. Hsu, Y.C. Chan, J.G. Duh, J.W. Lee, J.S.C. Jang, G.J. Chen, Antimicrobial properties of Zr–Cu–Al–Ag thin film metallic glass, Thin Solid Films 561 (2014) 98–101.
[20] Y.Y. Chu, Y.S. Lin, C.M. Chang, J.K. Liu, C.H. Chen, J.C. Huang, Promising antimicrobial capability of thin film metallic glasses, Mater. Sci. Eng. C Mater. Biol. Appl. 36 (2014) 221–225.
[21] W. Hou, S.B. Cronin, A review of surface plasmon resonance-enhanced photocatalysis, Adv. Funct. Mater. 23 (13) (2013) 1612–1619.
[22] Y.J. Lin, H.K. Lin, Y.H. Lin, Construction of Raman spectroscopic fingerprints for the detection of Fusarium wilt of banana in Taiwan, PLoS One 15 (3) (2020) e0230330.
[23] G. An, S. Li, W. Zhang, Z. Fan, Y. Bao, A polarization filter of gold-filled photonic crystal fiber with regular triangular and rectangular lattices, Opt. Commun. 331 (2014) 316–319.
[24] M.G. Albrecht, J.A. Creighton, Anomalously intense Raman spectra of pyridine at a silver electrode, J. Am. Chem. Soc. 99 (15) (1977) 5215–5217.
[25] E.C. Le Ru, P.G. Etchegoin, Quantifying SERS enhancements, MRS Bull. 38 (8) (2013) 631–640.
[26] J. Mun, D. Lee, S. So, T. Badloe, J. Rho, Surface-enhanced spectroscopy: Toward practical analysis probe, Appl. Spectrosc. Rev. 54 (2) (2019) 142–175.
[27] D. Lee, S. Yoon, Effect of nanogap curvature on SERS: a finite-difference time-domain study, J. Phys. Chem. C 120 (37) (2016) 20642–20650.
[28] S. Dodson, M. Haggui, R. Bachelot, J. Plain, S. Li, Q. Xiong, Optimizing electromagnetic hotspots in plasmonic bowtie nanoantennae, J. Phys. Chem. Lett. 4 (3) (2013) 496–501.
[29] C. Tabor, R. Murali, M. Mahmoud, M.A. El-Sayed, On the use of plasmonic nanoparticle pairs as a plasmon ruler: the dependence of the near-field dipole plasmon coupling on nanoparticle size and shape, Chem. A Eur. J. 113 (10) (2009) 1946–1953.
[30] Y.Y. Liang, X. Lin, M. Liang, F.C. Brunicardi, P. ten Dijke, Z. Chen, K.W. Choi, X. H. Feng, dSmurf selectively degrades decapentaplegic-activated MAD, and its overexpression disrupts imaginal disc development, J. Biol. Chem. 278 (29) (2003) 26307–26310.
[31] P. Ma, F. Liang, Y. Sun, Y. Jin, Y. Chen, X. Wang, H. Zhang, D. Gao, D. Song, Rapid determination of melamine in milk and milk powder by surface-enhanced Raman spectroscopy and using cyclodextrin-decorated silver nanoparticles, Microchim. Acta 180 (11–12) (2013) 1173–1180.
[32] N. Suresh Kumar, R. Padma Suvarna, K. Chandra Babu Naidu, P.P. Mohapatra, P. Dobbidi, X-band electromagnetic properties of hydrothermally synthesized La1-xBixTiO3 (x = 0.2–0.8) nanoparticles, Inorg. Chem. Commun. 149 (2023) 11408.
[33] A. Kumar, K.M. Gangawane, Synthesis and effect on the surface morphology & magnetic properties of ferrimagnetic nanoparticles by different wet chemical synthesis methods, Powder Technol. 410 (2022).
[34] H. Zheng, M.S. Matseke, T.S. Munonde, The unique Pd@Pt/C core-shell nanoparticles as methanol-tolerant catalysts using sonochemical synthesis, Ultrason. Sonochem. 57 (2019) 166–171.
[35] Y. Oh, M. Lee, Single-pulse transformation of Ag thin film into nanoparticles via laser-induced dewetting, Appl. Surf. Sci. 399 (2017) 555–564.
[36] Y. Oh, J. Lee, M. Lee, Fabrication of Ag-Au bimetallic nanoparticles by laser-induced dewetting of bilayer films, Appl. Surf. Sci. 434 (2018) 1293–1299.
[37] H.K. Lin, J.J. Wang, W.H. Lu, W.S. Chuang, C.Y. Chen, H.S. Chou, J.C. Huang, Microstructure and optical properties of AgCuAl medium entropy films with

nanoparticles induced by pulsed-laser dewetting, Surf. Coat. Technol. 421 (2021) 127427.
[38] N. Abid, A.M. Khan, S. Shujait, K. Chaudhary, M. Ikram, M. Imran, J. Haider, M. Khan, Q. Khan, M. Maqbool, Synthesis of nanomaterials using various top-down and bottom-up approaches, influencing factors, advantages, and disadvantages: a review, Adv. Colloid Interface Sci. 300 (2022) 102597.
[39] P. Pandey, S. Kunwar, J. Lee, Solid state dewetting of Ag/Pt bilayers for the stronger localized surface plasmon resonance (LSPR) properties: the dynamic control of surface morphology and elemental composition of AgPt and Pt nanostructures by the auxiliary Ag layer, J. Alloy. Compd. 813 (2020) 152193.
[40] A. Le Bris, F. Maloum, J. Teisseire, F. Sorin, Self-organized ordered silver nanoparticle arrays obtained by solid state dewetting, Appl. Phys. Lett. 105 (20) (2014) 203102.
[41] D. Wang, P. Schaaf, Solid-state dewetting for fabrication of metallic nanoparticles and influences of nanostructured substrates and dealloying, Phys. Status Solidi A 210 (2013) 1544–1551.
[42] P.D. Rack, Y. Guan, J.D. Fowlkes, A.V. Melechko, M.L. Simpson, Pulsed laser dewetting of patterned thin metal films: a means of directed assembly, Appl. Phys. Lett. 92 (22) (2008) 223108.
[43] S. Yang, F. Xu, S. Ostendorp, G. Wilde, H. Zhao, Y. Lei, Template-confined dewetting process to surface nanopatterns: fabrication, structural tunability, and structure-related properties, Adv. Funct. Mater. 21 (13) (2011) 2446–2455.
[44] F. Ruffino, A. Gentile, M. Zimbone, G. Piccitto, R. Reitano, M.G. Grimaldi, Size-selected Au nanoparticles on FTO substrate: controlled synthesis by the Rayleigh-Taylor instability and optical properties, Superlattice. Microst. 100 (2016) 418–430.
[45] Y. Kazakova, Y. Andreeva, M. Sergeev, V. Mikhailovskii, E. Ageev, Formation of nanoparticles from thin silver films under a liquid layer by single-shot nanosecond laser action, Opt. Quant. Electron. 52 (2) (2020) 97.
[46] S. Yadavali, R. Kalyanaraman, Nanomaterials synthesis by a novel phenomenon: the nanoscale Rayleigh-Taylor instability, AIP Adv. 4 (4) (2014) 047116.
[47] H.K. Lin, C.W. Huang, Y.H. Lin, W.S. Chuang, J.C. Huang, Effects of accumulated energy on nanoparticle formation in pulsed-laser dewetting of AgCu thin films, Nanoscale Res. Lett. 16 (1) (2021) 110.
[48] D.D. Evanoff Jr., G. Chumanov, Synthesis and optical properties of silver nanoparticles and arrays, ChemPhysChem 6 (7) (2005) 1221–1231.
[49] X. Liu, D. Li, X. Sun, Z. Li, H. Song, H. Jiang, Y. Chen, Tunable dipole surface plasmon resonances of silver nanoparticles by cladding dielectric layers, Sci. Rep. 5 (2015) 12555.
[50] J. Wang, Y. Hu, X. Yu, X. Zhuang, Q. Wang, N. Jiang, J. Hu, Recyclable and ultrasensitive SERS sensing platform: deposition of atomically precise Ag152 nanoclusters on surface of plasmonic 3D ZnO-NC/AuNP arrays, Appl. Surf. Sci. 540 (2021) 148324.
[51] M.A. Basyooni, A.M. Ahmed, M. Shaban, Plasmonic hybridization between two metallic nanorods, Optik 172 (2018) 1069–1078.